AIAA SciTech
4-8 January 2016, San Diego, California, USA
54th AIAA Aerospace Sciences Meeting

Design and Optimization of Short-Range Aluminum-Air Powered Aircraft

J. Michael Vegh*, Juan J. Alonso†
Stanford University, Stanford, CA, 94305, U.S.A.

Short-range, all-electric regional transport aircraft have been designed in an attempt to explore potential applications for carbon-free aircraft. The particular system of interest uses aluminum-air batteries, which have high specific energy characteristics (∼1300 W-h/kg), but lackluster specific power characteristics (∼.2kW/kg). Furthermore, these batteries are non-rechargeable, but have projected costs for both recycling as well as purchase of the consumed aluminum anode; this paper investigates optimization of these aircraft according to both weight and operating cost. Results suggest that these aircraft may be viable using essentially present-day technology, albeit with a significant weight penalty over comparable turboprop aircraft. Furthermore, at moderate design ranges, there are trade-offs between weight, operating cost, as well as field length. Operating costs are projected to be substantially lower than current aircraft at a variety of design ranges and further study is recommended.

Nomenclature

AoA	angle of attack
AR	aspect ratio
Esp	specific energy
F	Faraday Constant
h	altitude
f_{aux}	auxiliary power fraction
h_{frac}	altitude as fraction of cruise altitude
mgf	battery mass gain factor
P	power
Psp	specific energy
$\frac{t}{c}$	thickness to chord ratio
FL	Field Length
TOFL	Take Off Field Length
LFL	Landing Field Length
V	velocity magnitude
W	Weight
WL	wing loading
V_0	reaction potential
Λ	sweep
λ	taper ratio

Subscripts

1,2,3...	segment number
i	initial
f	final

*Ph.D. Candidate, Department of Aeronautics & Astronautics.
†Professor, Department of Aeronautics & Astronautics, AIAA Associate Fellow.

I. Introduction

The design of electric aircraft at the commercial scale has significant challenges, not least of which is due to the physical limitations of battery-based energy storage systems. These systems tend to not only be severely energy-constrained, but may also run into discharge-rate limitations. All-electric regional transport aircraft have been designed by the author using lithium-air batteries($\sim$ 2,000 W-h/kg, .66 kW/kg), with relatively modest weight penalties over comparable turbojet aircraft.[1] For reference, jet fuel has a specific energy $\sim$ 12,000 W-h/kg. Aluminum-air batteries are a recent topic of interest due to their impressive specific energy characteristics ($\sim$1300 W-h/kg) and high technology readiness level, but possess poor specific power ($\sim$ .2kW/kg). The given specific energy and specific power are representative of batteries produced in 2002.[2] A prototype electric car powered by a combination of aluminum-air and lithium-ion batteries has been developed and tested, with commercial production estimated in 2017.[3] The prototype car is pictured below.

Figure 1: Phinergy Prototype Aluminum-Air Car[4]

One drawback of aluminum-air batteries is difficulty in recharging the battery without a significant loss in capacity. A proposed economic model involves replacing and recycling the aluminum plates after discharge instead, which entails an estimated cost of \$1.1/kg of aluminum anode.[2] Like lithium-air batteries, aluminum-air batteries accumulate oxygen while discharging. In addition, unlike lithium-air batteries, aluminum-air batteries require water to operate, as seen by the aluminum-air chemical reaction below.

$$4Al + 3O_2 + 6H_2O \Rightarrow 4Al(OH)_3 + 2.71V \tag{1}$$

Any aircraft powered by aluminum-air batteries needs to carry the necessary water supplies, which must be accounted for in the sizing of the vehicle. This study investigates many of these trade offs, with a relative size chosen to be comparable to an Embraer 120, i.e. the target market is towards the regional turboprop scale. This aircraft configuration was chosen for a number of reasons; firstly, because of the relatively high technology readiness level of aluminum-air batteries, these aircraft may be able to enter the market more quickly. Secondly, these aircraft are closer in scale to electric vehicles from the automotive industry, which may enable the designer to leverage off-the-shelf components (such as electric motors and lithium-ion batteries), reducing development costs. Thirdly, the shorter range would appeal to a less crowded market than larger airliners such as the 737, which improves chances for commercial success. Finally, the direct operating cost for these aircraft would likely be smaller than equivalent gas-powered designs, due to the relatively low cost of electricity, along with more efficient energy conversion systems. Thus, their smaller size and scope could enable a comparatively early entrance of electric propulsion concepts into the commercial aviation market. On the other hand, aluminum-air batteries would function as primary batteries, and thus,

not be rechargeable. Therefore, they would have to be recycled onsite. Additionally, there is still a significant specific energy penalty vis. a vis. fossil fuels, which results in larger aircraft than turboprops of comparable performance. Furthermore, their poor specific power requires the incorporation of less energy dense, but more power dense lithium-ion batteries for high-power operation (such as climb), which results in additional design complexity.

Table 1 shows a summary of the cabin seating arrangement which is fixed for all configurations. The fuselage layout can be seen in Figure 2. The cruise velocity for the aircraft shown in this paper was a fixed 287 knots.

Table 1: Cabin and Fuselage summary

cabin length	31.2 ft.
seat pitch	32”
number of passengers	30
aisle width	21.75 ”
seat width	18”
tailcone fineness ratio	2
nose fineness ratio	1.5

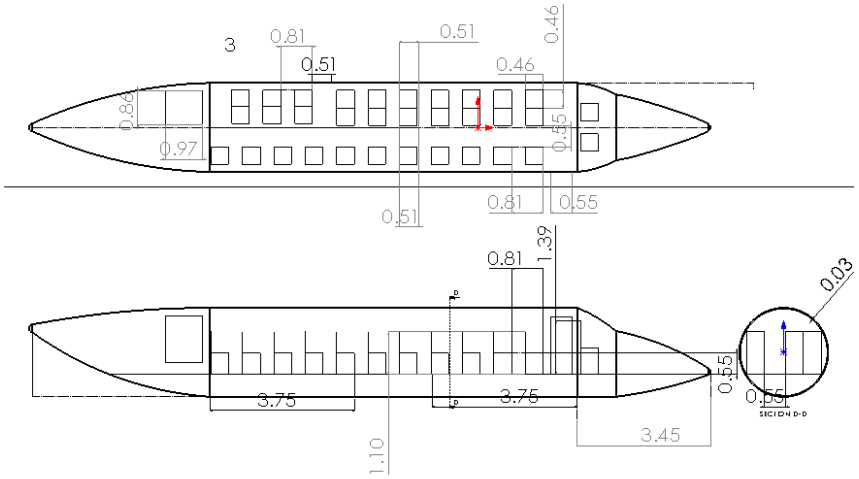

Figure 2: Fuselage Layout

II. Methodology

Electric Ducted Fans (EDFs) were selected as the propulsor of choice for these aircraft. Unfortunately, there are few EDFs at the scale required for this design (and fewer still are optimized for weight), and thus, additional assumptions must be made. Trade studies should be made as to the potential benefits of using twin, rather than quad-fan designs for these aircraft. Benefits of the quad fan include the fact that electric power is not as sensitive to scale as combustion-based systems,[5] and thus, these motor-based systems would not see as significant of a penalty from scaling as compared to using multiple smaller turbojets. Furthermore, the designer may be able to leverage automotive motor technology by using multiple, smaller EDFs, which are closer to what might one see in an electric car. However a four-EDF design may be undesirable due to mounting issues, as the wing was chosen to have extensive flap and slat area to accommodate expected issues with takeoff and landing constraints.

It may be advantageous to mount two EDFS on the tail as well as two EDFs on the wing, and this is the scheme chosen for this aircraft. This also has the added benefit of allowing for more flexibility in battery placement (in the event that the wings do not have enough volume to contain them), to control cg-travel during discharge. Perhaps more importantly, this reduces the engine-out thrust requirements for climb and takeoff, which is important both for reducing the overall size of each engine, as well as power demands on the motor and battery (remembering that aluminum air batteries are extremely power limited, with a specific power of about .2 kW/kg). Nacelle diameters were sized based on actuator disk theory, with an overall fan pressure ratio of 1.2. The electric motors as well as auxiliary lithium ion batteries were sized based on maximum power requirements in the mission using the sizing correlations shown below.

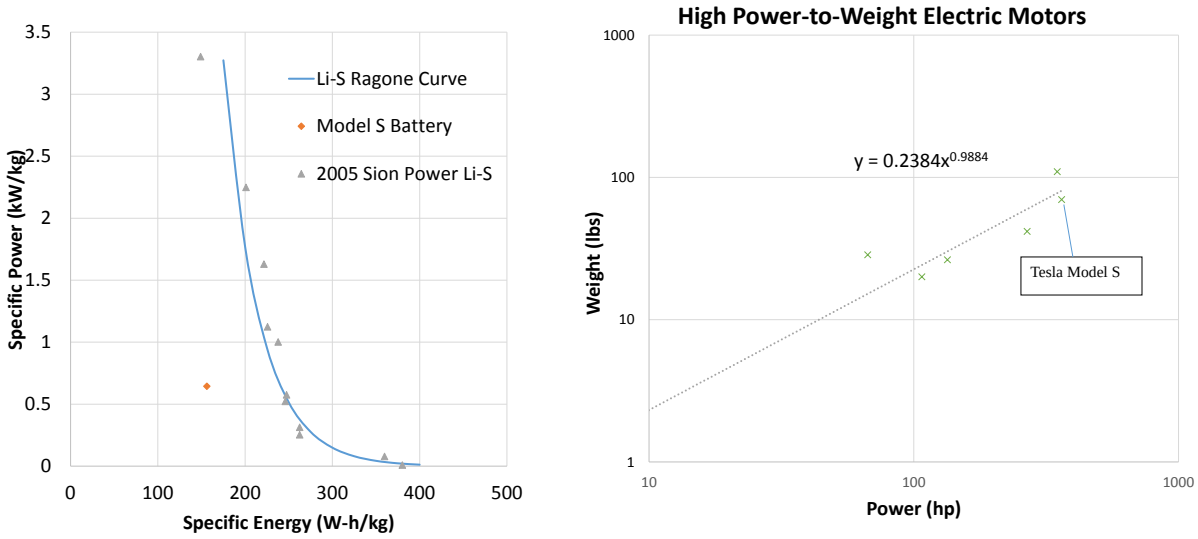

Figure 3: Auxiliary Battery Ragone Plot[6,7] /Electric Motor Scaling Correlation[8]

All aircraft in this paper were designed using the curve fit in Figure 3 to determine electric motor mass. Additionally, the auxiliary battery weight was determined based on the 2005 lithium-sulfur plot in Figure 3;[6] this was assumed to be representative of near-term lithium-ion technology, with the current Tesla Model S battery plotted alongside the curve.[7] Note that, at the cell level, the Tesla Model S battery has a specific energy of 233 W-h/kg, corresponding to a battery specific energy of about 65 % that of the cell level.[9] Recent studies have produced lithium-ion cells at 350 W-h/kg while retaining 80 % capacity for 500 cycles.[10] Assuming a 65 % packaging efficiency and similar specific power to the Tesla Model S battery, this results in battery characteristics comparable to the Li-S curve in Figure 3. Aluminum-air mass properties were determined from the curve in Figure 4, which was produced from the discharge profile curve taken from reference 2. The original discharge curve is repeated in Figure 5 below.

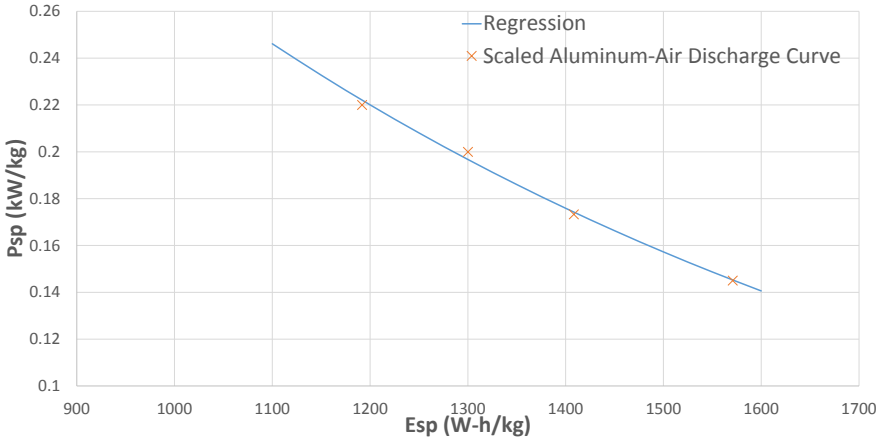

Figure 4: Aluminum-Air Ragone Curve

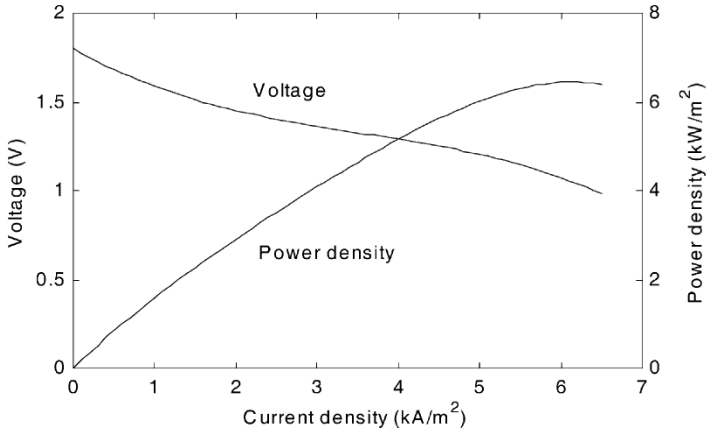

Figure 5: Aluminum-Air Cell Discharge Curve[2]

Figure 4 was produced by scaling the discharge properties from Figure 5; a nominal specific energy of 1300 W-h/kg, specific power of .2 kW/kg, and voltage of 1.2 volts was assumed. From the nominal voltage and specific energy, the nominal capacity in A-h/kg was determined. This was used to determine the discharge time in h/kg from Figure 5, which was multiplied by the power density to find the specific energy in W-h/kg-m^2; the entire curve was then scaled from the nominal voltage, and plotted, producing Figure 4. The primary battery was sized from this curve, based on the energy and power demands, and was bounded between an Esp of 1100 and 1600 W-h/kg.

Battery discharge losses were modeled using an empirical model developed in reference 11. Additionally, the mass gain rate of the aircraft from battery discharge was based on the cathode half cell reaction (equation 2).

$$O_2 + 2H_2O + 4e^- \Rightarrow 4OH- + .4V \tag{2}$$

The mass gain rate is then simply

$$\dot{m_{O_2}} = \frac{MW_{O_2}}{4V_{4AL(OH)_3}} \cdot F \cdot P \tag{3}$$

where the factor of four comes from the cathode half-reaction. Water consumption is also based on the cathode half cell reaction, and is shown below

$$m_{H_2O} = \frac{MW_{H_2O}}{2V_{4AL(OH)_3}} \cdot F \cdot E \tag{4}$$

Finally, in order to properly evaluate the F, the mass of the aluminum can be calculated from the half cell reaction below.

$$Al + 3OH- \Rightarrow Al(OH)_3 + 3e^- - 2.31V \tag{5}$$

$$m_{Al} = \frac{MW_{Al}}{3V_{4AL(OH)_4}} \cdot F \cdot E \tag{6}$$

With a 1.1$/kg cost of operation to replace the aluminum anode, one can use these equations to estimate not only the proportional system-level weight of the battery including oxygen and water, but also overall cost of operation. Assuming the national average price for electricity of 12 cents/kW-h, along with the average water cost of .04 cents/kg, one can determine the operation cost from the energy requirements of the mission. Furthermore, one can calculate the overall systems-weight requirements of an aluminum-air battery; both are shown below, along with a representative cost comparison for jet fuel, based on a 30% overall energy conversion efficiency and the national average cost of jet fuel of $4.36/gallon.[12]

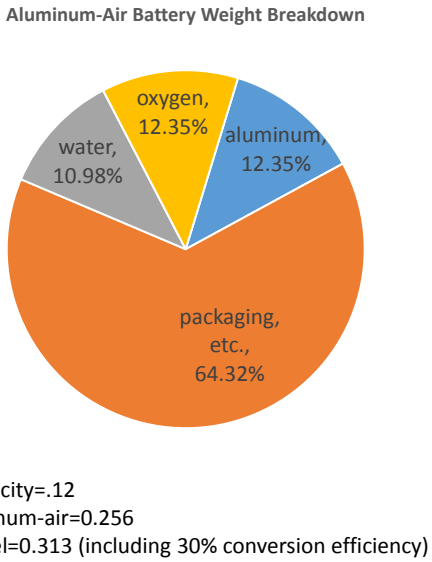

Figure 6: Aluminum-Air Battery Cost and Weight Breakdowns

Other component weights were estimated based on traditional sizing correlations in SUAVE, details of which can be seen in reference 13. Note that a 20% tech factor was used for wing weight to model the incorporation of composites, along with load alleviation from placing the batteries along the span of the wing. Aerodynamic properties were calculated via a weissinger vortex lattice method with profile drag correlations. Physical design variables for the aircraft are shown in Table 2, while mission trajectory design variables are shown in Table 3. Climb and descent profile characteristics that were fixed across all configurations are shown in Table 5 in the Appendix.

Table 2: Aircraft Design Variables

variable	Lower Bound	Upper bound
f_{aux}	0	1.
AR	5	14
WL	$200\frac{kg}{m^2}$	$800\frac{kg}{m^2}$
λ	.1	.3
$\frac{t}{c}$	.07	.2

Table 3: Mission Design Variables

variable	Lower Bound	Upper bound
V_{climb_1}	$50\frac{m}{s}$	$140\frac{m}{s}$
V_{climb_2}	$50\frac{m}{s}$	$140\frac{m}{s}$
V_{climb_3}	$50\frac{m}{s}$	$140\frac{m}{s}$
h_{cruise}	20,000 ft.	30,000 ft.
$h_{frac,climb_1}$	.1	1
$h_{frac,climb_2}$	.2	1
$h_{frac,descent_1}$	.1	1

Design variables were constrained to limit required field lengths, ensure a reasonable angle of attack, as well as ensure consistency in the flight profile. The constraints can be seen below.

$$h_{frac,climb_1} < h_{frac,climb_2} \tag{7}$$

$$-15^\circ \leq AoA \leq 15^\circ \tag{8}$$

$$TOFL \leq 2500ft \tag{9}$$

$$LFL \leq 2500ft \tag{10}$$

$$throttle \leq 1 \tag{11}$$

Vehicles were evaluated using SUAVE, an open-source aircraft design framework.[13] Optimization was handled using pyOpt, courtesy of SUAVE's pyOpt optimizer wrapper, which was used to call SNOPT.[14,15] Battery operation was handled as follows: the primary battery meets all of the power demands up to its maximum available power, at which point the auxiliary battery kicks in and meets any additional power demand. If the guesses for total energy requirements or weight were not equal to the outputted values to within a specified tolerance (in this case 1%), or the auxiliary battery was discharged beyond its total energy capacity, a new guess was initialized, until the sizing loop converged.

III. Results

The inclusion of the auxiliary lithium-ion battery was crucial in permitting closure of the aircraft designs. Additionally, the power system was quite unusual, in that, although the aluminum-air battery was very large, it was still power, rather than energy-constrained; in fact, below the 1150 nautical mile design range, the aircraft did not carry enough water to fully discharge the battery, but instead, requires a large aluminum-air battery mass in order to meet power demands while discharging only a fraction of the total energy; this

may be alleviated somewhat by clever rearrangement of the battery cells, but may prove more difficult as plumbing systems are required to deliver the air and water to each of them. The auxiliary lithium-ion battery greatly alleviates this, but in most cases, the primary battery is not fully discharged at the end of the mission. For instance, depending on the aircraft, the primary battery state of charge at the end of the mission may be as high as .5. Figures 7 and 8 below illustrate pareto fronts of aircraft landing weight and operating cost vs. design range along with comparable fronts where the field length requirement is relaxed to 5,000 ft (noting that the maximum field length seen in these designs was about 4,100 ft). The Embraer 120 is also shown, based on its design range and fuel capacity, assuming a jet fuel cost of $ 4.36/gallon (the 2015 national average).[12,16]

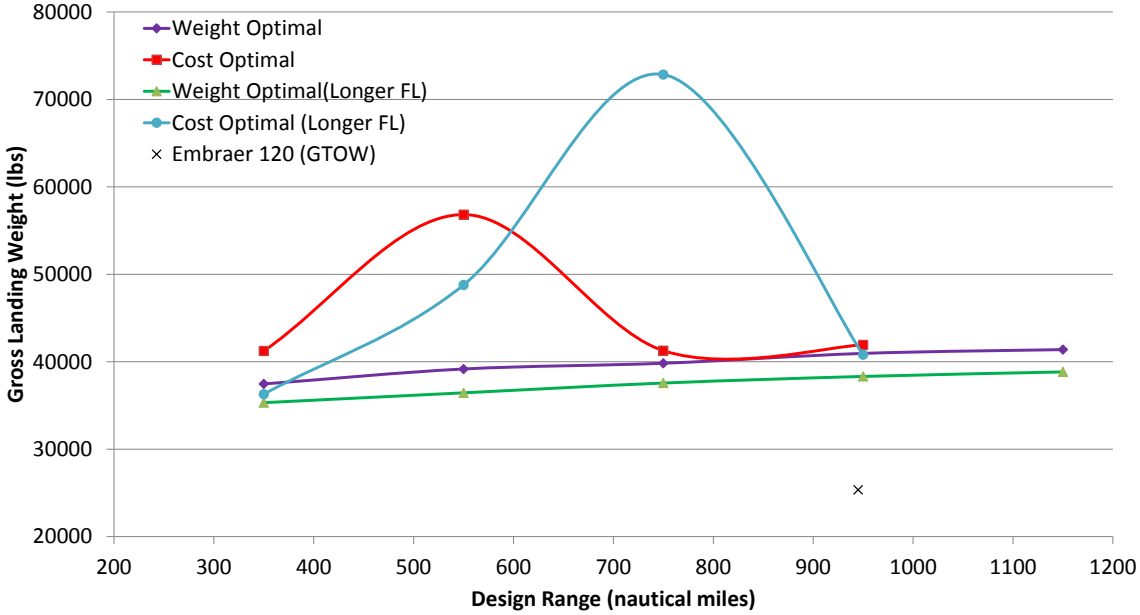

Figure 7: Weight Pareto Fronts

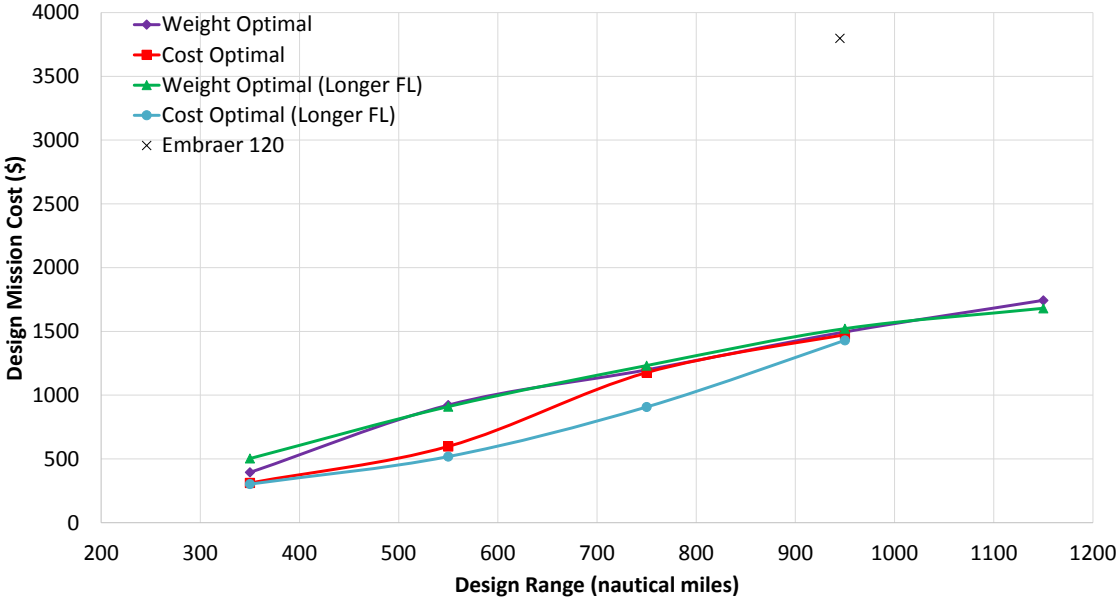

Figure 8: Cost Pareto Fronts

For the 2,500 ft. field length designs, the optimizer tended to close on aircraft with the highest wing loading possible without violating any of the constraints. As one might expect, relaxing these constraints led to higher wing loadings. For both extremely short range aircraft, as well as aircraft with design ranges longer than ∼900 nautical miles, the weight optimal and cost optimal designs correlate strongly with each other. This is primarily a result of f_{aux} variation. To illustrate, for the same amount of energy, a lithium-ion battery costs roughly half as much to operate as an aluminum-air battery (see Figure 6), albeit at about eight times the weight. The cost optimal designs tended towards battery auxiliary power fractions of 1 below a ∼800 nautical mile design range, while the propulsion system for the weight optimal design transitions to primarily aluminum-air at 500 nautical miles.

All of the aircraft shown here possess a significantly smaller operating cost than the Embraer 120. On the other hand, all of the aircraft are considerably heavier (about 1.5 times the weight at comparable range). This is because even the impressive specific energy of the aluminum-air battery is still less than 1/6 that of jet fuel, and comes with a number of other power supply issues. When including the energy conversion efficiency, the effective specific energy remains less than 35 % that of Jet A. However, due to the lower cost of electricity, these aircraft do offer strong potential economic benefits, which may cause them to merit further consideration. Table 4 shows a summary of results for weight optimal and cost optimal aircraft, based on a design range of 950 nautical miles.

Table 4: Optimization Results (Design Range=950 Nautical Miles)

variable	Weight Optimal	Cost Optimal	Weight Optimal (Relaxed Field Length)	Cost Optimal (Relaxed Field Length)
f_{aux}	.217	.278	.239	.246
AR	14	14	14	14
$WL\frac{kg}{m^2}$	338	316	558	372
λ	.1	.1	.1	.1
$\frac{t}{c}$	.168	.135	.149	.111
$V_{climb_1}(\frac{m}{s})$	67.1	67.6	77.5	77.1
$V_{climb_2}(\frac{m}{s})$	80.5	72	85.6	77.2
$V_{climb_3}(\frac{m}{s})$	92.0	93.2	95.0	97.3
h_{cruise} (ft.)	28,500	29,300	20,000	27,500
$h_{frac,climb_1}$	.12	.17	.17	.10
$h_{frac,climb_2}$	.20	.20	.20	.20
$h_{frac,descent_1}$	.13	.37	.43	.38
Field Length(ft)	2,500	2,500	4,100	3,100
GLW (lbs.)	40,830	41,950	38,330	40,800
Operating Cost ($)	1,497	1,475	1,521	1,431

Cost optimal designs tended to possess lower wing loadings, higher design altitudes, as well as higher climb velocities. Furthermore auxiliary power fractions were higher for the cost-optimal aircraft, which, due to the higher climb velocities, caused a higher fraction of total energy requirements to come from the lithium-ion battery. In addition, the optimizer closed on aircraft with the minimum taper ratio and maximum aspect ratio. Figure 9 shows a comparison of the operating cost/passenger-mile of these aircraft, along with some representative regional transport aircraft using the same assumptions outlined above (i.e. fuel cost/gallon= $ 4.36).

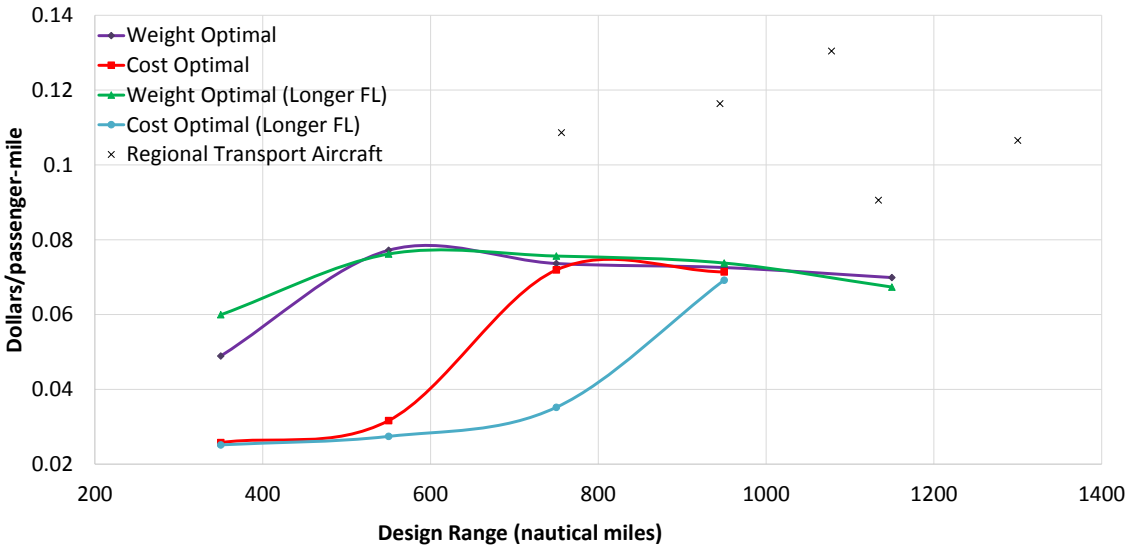

Figure 9: Cost/Passenger Mile Pareto Fronts

Figure 9 illustrates that these aircraft, while suffering from a significant weight penalty over more traditional turboprop aircraft, offer substantial economic benefits, even when including the cost of recycling the aluminum. Furthermore, outside of the all lithium-ion ranges, the aircraft operating cost/passenger-mile curves for the most part scale flatly vs. design range. The exception is the weight optimal, longer field length curve, which shows favorable scaling at longer ranges. This suggests that these aircraft may be economically profitable at a variety of design ranges. Thus, one could potentially design an aircraft for a longer range, while replacing the battery system at the airport with whatever combination of aluminum-air and lithium-ion batteries minimizes the operating cost for that particular mission.

Now, with battery weight consuming a much larger portion of the aircraft than fuel weight does in modern commercial aircraft, volumetric issues may arise in battery and water placement. Figure 10 illustrates a potential schematic, which highlights a proposed layout for the required battery and water storage, along with some span issues for the shorter-field length designs.

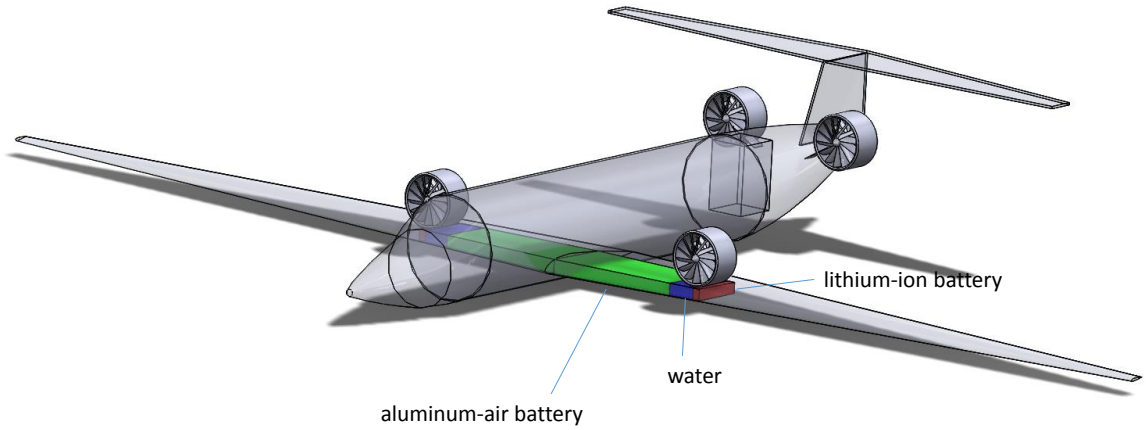

Figure 10: Aircraft Schematic (950 nautical miles)

Even though this aircraft possesses an extremely large primary battery (taking up about 30% of the gross landing weight of the aircraft), its high density (assumed to be comparable to the Tesla Model S battery[9]) reveals that volumetric constraints appear to not be a critical issue in these aircraft. Nonetheless, the wingspan of the shorter field-length designs are too large for an aircraft of this configuration, and would be unfeasible to produce. However, relaxing the field length not only leads to lighter designs, but also more reasonable span lengths, due to the higher wing loading, as seen in Figure 11.

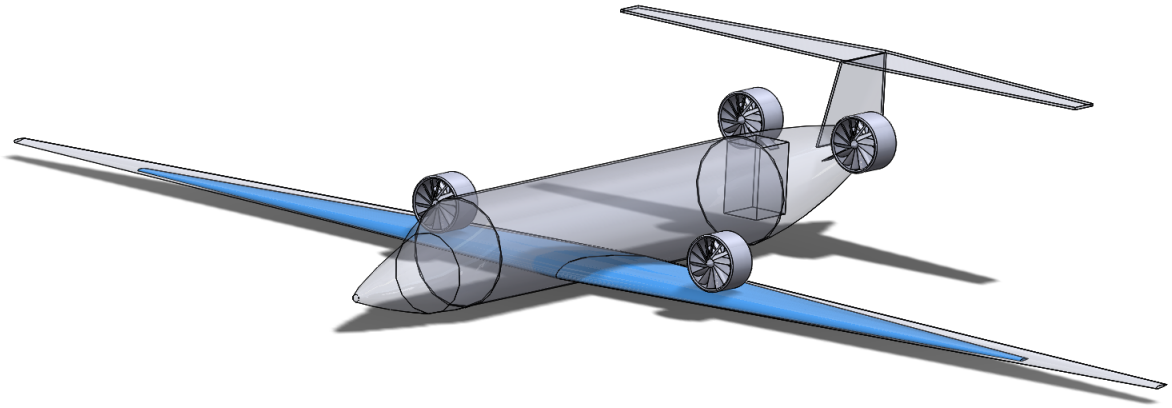

Figure 11: Aircraft Wing Comparison (950 nautical miles)

While Figure 11 illustrates a more reasonable-looking (and lighter) aircraft, the reduced wing area raises questions about potential volumetric limitations. To that end, Figure 12 shows the relaxed field length design, together with the wing volume required to house the batteries and water.

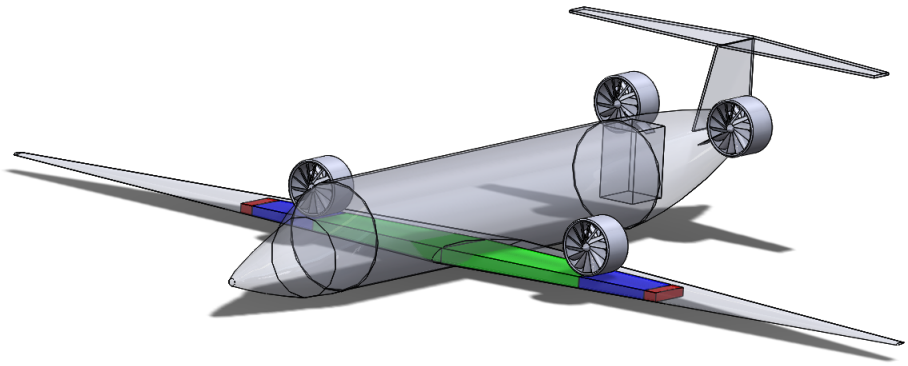

Figure 12: Relaxed Field Length Aircraft (950 nautical miles)

Figure 12 demonstrates that, while the longer-field length designs possess considerably less room for the energy systems than the more field-constrained designs, they appear to remain a non-issue. Figure 13 shows the weight breakdowns for the 950 nautical mile, relaxed field length designs, allowing the reader a more complete understanding of the tradeoffs between cost and weight.

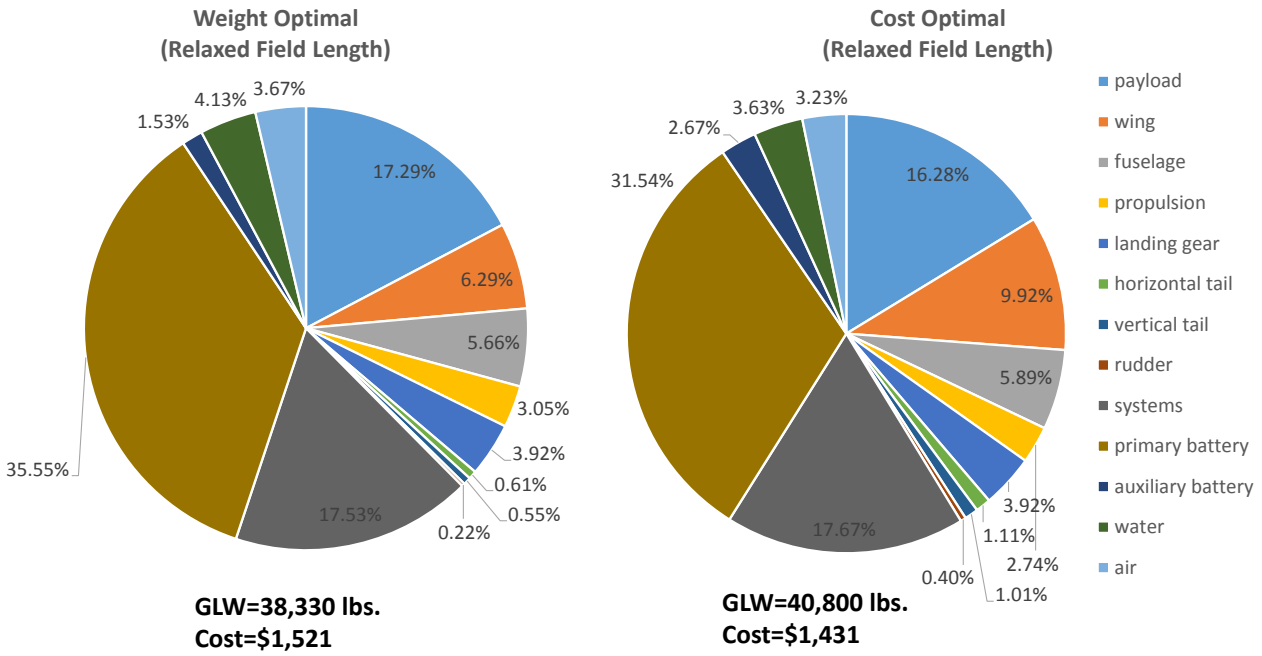

Figure 13: Weight Breakdowns (950 nautical miles)

As Figure 13 shows,the primary battery takes up a considerable percentage of the overall aircraft weight, especially in the weight optimal cases. The cost optimal aircraft on the other hand trade aluminum-air battery weight for structural and lithium-ion battery weight, which results in a further weight penalty albeit with modest gains in operating cost.

Any implementation of this technology across would likely be gradual, and therefore, there would be cases where the aluminum hydroxide could not be recycled onsite. Thus, it is important to determine the operating cost not only when economical aluminum recycling happens near the airport, but also when aluminum must be purchased directly. To that end, the chart in Figure 9 is rescaled based on an estimated purchasing cost of $2.33/kg of refined aluminum and shown below.[2]

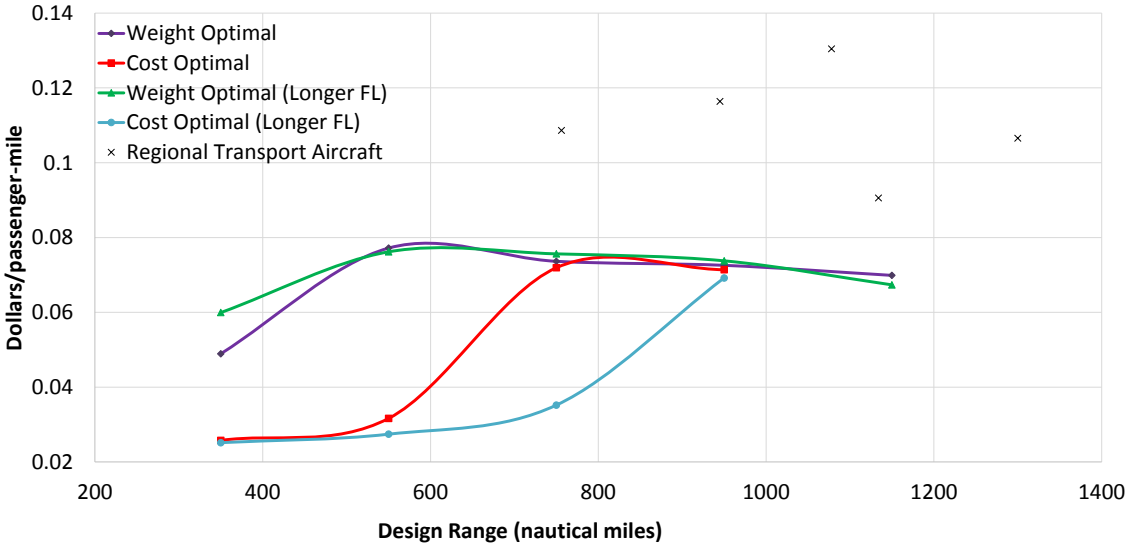

Figure 14: Operating Cost Without Recycling

Despite a significant spike in the aluminum price, these aircraft continue to perform somewhat more efficiently than other regional transport aircraft, at least from an operating cost standpoint. Thus, an early market entry of these designs, even without the recommended aluminum recycling infrastructure may allow for lower operating costs over current aircraft. Nonetheless, substantial weight penalties exist over comparable turboprops, which suggests that their unit price would be higher than similar gas-powered aircraft. The new technology and novel configuration would only compound this. Furthermore, the data here does not include labor, which would bring the operating cost curves closer to the other transport aircraft.

On the other hand, in looking forward, one could theoretically build an airframe for the longest desirable operating range, while loading different combinations of aluminum-air and lithium-ion batteries to reduce operating costs. This could substantially reduce ticket prices while simultaneously increasing the airline profit margins. For instance, one can design an aircraft for a maximum range of up to 1150 nautical miles, but only load it with lithium-ion batteries for mission ranges below 300 nautical miles. This would require a detailed database for the airline and airport, but could substantially reduce operating cost even at the initial entry into service while allowing for a large degree of mission flexibility.

IV. Conclusions

The work reveals that, for the missions here, advanced aluminum-air batteries are severely power-constrained. Including lithium-ion batteries within the aircraft is crucial in allowing the sizing loop to close, and results in a number of interesting aircraft characteristics. For instance, between ∼500 and ∼800 nautical miles, the cost optimal designs tended towards all lithium-ion aircraft, with significant weight penalties, while the weight optimal designs transitioned quickly to larger proportions of aluminum-air. Furthermore, while these aircraft possessed significant weight penalties vs. turboprop designs of comparable performance, their operating cost was significantly smaller. Span issues indicate that the baseline designs are not really worth investigating further; however, the longer field length designs show some promise, with significant cost benefits, even when purchasing the aluminum outright (rather than recycling). Thus, these aircraft configurations may be worth further study.

Acknowledgments

Michael Vegh would like to acknowledge the support of the DoD through the Science Mathematics and Research for Transformation (SMART) Scholarship Program.

References

[1]Vegh, J., Alonso, J., Orra, T., and Ilario da Silva, C., "Flight Path and Wing Optimization of Lithium-Air Battery Powered Passenger Aircraft," *AIAA 2015-1674 53rd AIAA Aerospace Sciences Meeting*, AIAA Scitech, Kissimee, FL, 2015.

[2]Yang, S. and Knickle, H., "Design and analysis of aluminum/air battery system for electric vehicles," Journal of Power Sources, 2002.

[3]Hruska, J., "New aluminum air battery could blow past lithium-ion, runs on water," Extreme Tech, Accessed: Mar. 15, 2015.

[4]Voelcker, J., "Phinergy 1000-Mile Aluminum-Air Battery: On The Road In 2017?" http://www.greencarreports.com/, 2013, Accessed: Oct. 26, 2015.

[5]Moore, M. and Fredericks, B., "Misconceptions of Electric Propulsion Aircraft and their Emergent Aviation Markets," *AIAA SciTech*, NASA Langley Research Center, National Harbor, Maryland, 2014.

[6]Affinito, J., "Developing Li-S Chemistry for High-Energy Rechargable Batteries," *Symposium on Scalable Energy Storage Beyond Li-Ion: Materials Perspectives*, Sion Power, Oak Ridge National Laboratory, 2010,.

[7]Roper, L., "Tesla Model S," http://www.roperld.com/science/TeslaModelS.htm, Accessed: Oct. 2015.

[8]Morris, C., "Elon Musk: Cooling, not power-to-weight ratio, is the challenge with AC induction motors," Charged: Electric Vehicle Magazine, 2014, https://chargedevs.com/, Accessed: Nov. 2, 2015.

[9]Menahem, A., "The Tesla Battery Report: Tesla Motors: Battery Technology, Analysis of the Gigafactory, and the Automakers' Perspectives," Tech. rep.

[10]Sinkula, M., "Transformative Vertical Flight Concepts," Tech. rep.

[11]Datta, A. and Johnson, W., "Requirements for a Hydrogen Powered All-Electric Manned Helicopter," NASA Ames Research Center, Moffett Field, CA, 2011.

[12]"Fuel Price Report: Summary of Fuel Prices at 3655 FBOS nationwide," AirNav, https://www.airnav.com/fuel/report.html, accessed Nov. 5, 2015.

[13]Lukaczyk, T., Wendorff, A., Botero, E., MacDonald, T., Momose, T., Varyar, A., Vegh, J., Colonno, M., Orra, T., Illaria da Silva, C., and Alonso, J., "SUAVE: An Open-Source Environment for Multi-Fidelity Conceptual Vehicle Design," AIAA Aviation Forum 2015, Dallas, TX, 2015.

[14]Perez, R. E., Jansen, P. W., and Martins, J. R. R. A., "pyOpt: A Python-Based Object-Oriented Framework for Nonlinear Constrained Optimization," *Structures and Multidisciplinary Optimization*, Vol. 45, No. 1, 2012, pp. 101–118.

[15]Gill, P. E., Murray, W., and Saunders, M. A., "SNOPT: An SQP algorithm for large-scale constrained optimization," *SIAM Journal on Optimization*, Vol. 47, No. 1, 2002, pp. 99–131.

[16]"Embraer 120 Brasilia Airport Planning Section 11: General Airplane Characteristics," Embraer, http://www1.embraer.com/english/content/aeronaves/doc/SECTION02.PDF, accessed Nov. 5, 2015.

V. Appendix

Table 5: Constraints for Optimization Study

Climb/Descent Rates			**Descent Velocity Magnitudes**		
Climb 1	=	6 $\frac{m}{s}$	Descent 1	=	120 $\frac{m}{s}$
Climb 2	=	6 $\frac{m}{s}$	Descent 2	=	100 $\frac{m}{s}$
Climb 3	=	3 $\frac{m}{s}$			
Descent 1	=	5 $\frac{m}{s}$			
Descent 2	=	5 $\frac{m}{s}$			